Deepwater Channel Systems in the Orca and Choctaw Basins, Northern Gulf of Mexico

THESIS

Presented in Partial Fulfillment of the Requirements for the Degree Master of Science in the Graduate School of The Ohio State University

By

Katie Treiber

Graduate Program in Earth Sciences

The Ohio State University

2017

Master's Examination Committee:

Derek Sawyer, Advisor

Ann Cook

Michael Wilkins

Abstract

Turbidite channels are important conduits of clastic sediments into the deep ocean, with coarser-grained deposits creating potential reservoirs for hydrocarbons. In this study, three-dimensional seismic data and borehole logs from three industry wells were used to interpret channel systems, lithology, and overall depositional trends in the Orca and Choctaw mini-basins, located on the outer continental slope in the Gulf of Mexico in ~1645-2470 m (5400-8400 ft) of water. These mini-basins have previously been shown to have strong indications of gas hydrate in core samples and geophysical data, and the primary goal of this study was to identify coarse-grained sediments within channel systems that could serve as potential hydrocarbon reservoirs. To accomplish this, thirty-five channels were mapped in the ~2900 m (9500 ft) of sediment between the seafloor and top of salt. Channels were grouped into two broad morphological types to predict where coarse-grained sediments within each system were likely to occur. Basin depositional trends were also assessed to show how progressive salt withdrawal impacts channel occurrence by shifting topographic lows, in turn influencing where coarse-grained sediments are ultimately deposited. This research provides a detailed assessment of the turbidite channel systems in the Orca and Choctaw basins, and serves as model for

future studies using seismic and well log analysis to interpret turbidite channel systems in deepwater basins.

Acknowledgments

I would like to thank the contributing members of the Genesis of Methane Hydrate in Coarse-Grained Systems: Northern Gulf of Mexico Slope (GOM^2) project, funded by the U.S. Department of Energy (grant number: DE-FE0023919). The seismic data used in this study was collected and processed by WesternGeco, with well data provided by Unocal/Chevron. Bathymetry data from the Bureau of Ocean Energy Management was also used in this study. Sincere thanks to my advisor, Derek Sawyer, and committee members and mentors Ann Cook and Mike Wilkins. I would also like to thank my research group for their support, and The Ohio State University's School of Earth Sciences for their continued dedication to advancing the geological sciences.

Vita

May 1998 .....Thomas Jefferson High School

2012.....B.L.S., Iowa State University

2015.....B.S. Geology, Iowa State University

2015 to present .....Graduate Teaching Associate / Graduate Research Associate, School of Earth Sciences, The Ohio State University

Fields of Study

Major Field: Earth Sciences

Table of Contents

List of Tables

List of Figures

Introduction

Salt-withdrawal mini-basins are a major component of the bathymetry observed in the northern Gulf of Mexico (Jiang et al., 2012; Madof et al., 2009; Pilcher and Blumstein, 2007). These mini-basins create natural structural traps that have been successfully exploited by the oil and gas industry (Alexander and Flemings, 1995; BOEM, 2012). Turbidite channel systems also play an important role in hydrocarbon exploration in the Gulf of Mexico (Weimer and Link, 1991). These channels provide a conduit for coarser-grained terrestrial sediments to reach the deeper waters of the continental slope, and serve as potential reservoirs within more fine-grained marine sediments (Hubbard et al., 2014, Mayall et al., 2006; Hadler-Jacobsen et al., 2005).

While few studies have been published on the Choctaw Basin, focus has previously been placed on the Orca Basin due to an unusual brine pool covering a large portion of the basin. The brine pool was formed by the extrusion of salt on the flanks of the basin, creating more saline, denser waters that settled over approximately 123 km^2 (47.5 mi^2) of the basin floor (Pilcher and Blumstein, 2007). The density difference between the brine pool and the overlying water column is sufficient to create a prominent reflection in seismic data, and a majority of previous studies on the Orca Basin have focused either on the brine pool or on shallow (less than 12 mbsf) sediments in its

vicinity (Trabant and Presley, 1978; Tomkins and Shephard, 1979; Addy and Behrens, 1980; Pilcher and Blumstein, 2007; Tribovillard et al., 2008; Shokes et al., 1977). Little has been published on the deeper subsurface sediments, however, and a detailed interpretation of the sedimentological features and history of the basin has been largely undescribed.

The study area also merits interest as a known location for gas hydrate. Gas hydrate forms when a natural gas molecule, in the presence of water and at sufficiently low temperatures and high pressures, becomes trapped in a lattice of ice (Sloan, 2003). Gas hydrate has been linked to submarine landslides and global warming; it has also been recognized as an unconventional hydrocarbon resource of enormous potential (Birchwood et al., 2010; McConnell and Kendall, 2003; Kvenvolden, 1993). A recent global assessment of the amount of gas considered recoverable from hydrates is ~3 x 10^{14} m^3 (10^{16} ft^3) (Boswell and Collett, 2010).

The energy potential of gas hydrate makes locating hydrate in coarse-grained sediments particularly important. As with conventional oil and gas, higher reservoir permeability increases the technical producibility of hydrocarbons contained in the hydrate structure (Boswell and Collett, 2010). Grain-size also exerts a primary control on hydrate morphology and occurrence (Malinverno, 2010), influencing potential recovery. In fine-grained sediments, hydrate typically occurs in fractures or as small disseminated grains, while coarser-grained sediments generally have a more massive, pore-filling morphology (Clennel et al., 1999). This massive habit adds an economic benefit to targeting hydrates in coarse-grained reservoirs.

This study seeks to identify channel systems in the Orca and Choctaw basins using a combination of well log and 3-D seismic analysis to pinpoint where coarse-grained sediments are distributed. Basin-scale depositional trends are also analyzed to create a broad sedimentological history for the study area from seafloor to top of salt.

Geologic Setting

The Orca and Choctaw mini-basins are located on the continental slope approximately 250 km (155 miles) south of the Louisiana coastline in the northern Gulf of Mexico (**Fig. 1**). The water depth in the study area ranges from a maximum of 2470 meters (8100 feet) in the syncline of the Orca Basin to a minimum of 1645 meters (5400 feet) along the basin ridges, with slopes in the Orca Basin ranging from 2.5-22° (Pilcher and Blumstein, 2007). Sediments in the basins were sourced from the Mississippi River delta and range in age from the Miocene to the Holocene (Hillman et al., 2017; DSDP Vol. 96, Site 618; Trabant and Presley, 1978).

The Orca and Choctaw basins were created by the coupled processes of salt rise and sediment subsidence, as described in Pilcher and Blumstein (2007). Areas of increased sediment load cause expulsion of the underlying allochthonous salt canopy into areas of lower overburden pressure, where salt-cored anticlines form the ridges of the modern basin. Concurrently, synclinal areas of maximum load progressively subside and create accommodation as long as salt continues to withdraw.

This continued subsidence and uplift led to the enclosure of the Orca Basin, and the eventual formation of its unusual brine pool. Salt uplift along the ridges of the modern basin caused overlying sediments to slump, exposing the salt to seawater (Pilcher

and Blumstein, 2007). More saline, denser waters formed at these exposures and sunk to the seafloor, where the enclosed basin caused these waters to pool. Cores collected from the basin in 1975 showed interstitial pore waters had eight times the salinity of seawater, and a subsequent shallow seismic survey conducted a year later first imaged the prominent reflection between the brine pool and the overlying seawater (Trabant and Presley, 1978). This feature and the unusually high salinities in core samples attracted much of the early attention to Orca Basin.

Gas hydrate was first reported in the Orca Basin during Expedition 96 of the Deep Sea Drilling Project, where two holes drilled at Orca Site 618 identified hydrate in a number of core samples (DSDP Vol. 96, Site 618). Subsequent holes drilled by Unocal/Chevron in 2011-2013 noted possible gas hydrate in the drilling reports, and accompanying well logs showed resistivity spikes indicative of gas hydrate within the temperature and pressure-defined hydrate stability zone. Gas hydrate is also indicated by a strong but discontinuous bottom-simulating reflector (BSR) in three-dimensional seismic data (Kou et al., 2007; Hillman et al., 2017). The BSR forms at the base of the hydrate stability zone, below which higher temperatures prevent the frozen hydrate structure from forming. Seismic waves slow when traveling from the frozen hydrate-bearing sediments in the stability zone to free gas in the pore space below, creating a seismic reflection that often crosscuts stratigraphic reflections (Hillman et al., 2016; Birchwood et al., 2010).

Methodology

The interpretation in this study was based on seismic data and borehole logs from three industry wells. The three-dimensional seismic dataset spans 198 km^2 (76.5 mi^2) across the southern Orca and northern Choctaw basins **(Fig. 2)**. The seismic was acquired in 2009 by WesternGeco and processed using an anisotropic Kirchhoff depth migration. The cube was received post migration with a 5 meter (16 foot) sample rate and was interpreted using a near-zero phase rotation with American polarity.

The basic techniques and workflow used to interpret channel systems in the seismic data are described by Posamentier et al., 2007. To begin, multiple lines were taken through the seismic cube to manually pick channel segments visible in cross-section. Twelve laterally continuous horizons were then mapped across the study area to create stratal slices **(Fig. 3)**. These slices parallel mapped horizons and allow the interpreter to view the seismic data at a single geologic time, as opposed to depth slices that may cross-cut multiple stratigraphic reflections. To improve accuracy, a majority of horizons were mapped line by line to avoid misinterpretations from faults and the cross-cutting BSR. Once slices were created, amplitude extractions were used to identify additional channels in plan view.

Horizon probes were also created from the stratal slices to aid in interpretation. Probes parallel mapped horizons, but can be moved up and down through the seismic cube. They allow the interpreter to see an adjustable vertical 'window' of stacked amplitudes, a helpful technique in differentiating channel fill and overbank deposits. Opacity was applied to heighten the amplitudes of interest, in this case acoustically soft amplitudes that generally correspond to sands (Hadler-Jacobsen et al., 2005).

A coherence cube was also created from the 3-D seismic data to detect dissimilarities between seismic traces. Trace dissimilarities correspond to reflection edges and have been used to enhance stratigraphic features and delineate faults (Chopra and Pickford, 2001; Marfurt et al., 1998; Bahorich and Farmer, 1995). In this study, coherence was viewed on both depth slices and stratal slices to better distinguish channel margins. An attempt was also made to co-render the coherence and amplitude attributes, but the low relief of many of the channel systems made this technique ineffective.

Wells logs from three industry wells were used to ground the seismic interpretation. The primary logs studied were a gamma ray and resistivity log (A40L) to interpret lithology and fluid fill. In a final step, mapped horizons were flattened in profile-view to study the shape of the basin at time of deposition. Flattening was conducted in multiple directions to capture variations in uplift timing between ridges. Isopachs were also created to highlight changes in maximum accommodation position and overall depositional trends.

Seismic Overview

The Orca and Choctaw basins are characterized by largely isopachous reflections of variable amplitude. Heavy normal faulting occurs along the flanks of the basin, with small-scale listric faults in the shallow portion of the northern Choctaw syncline. Prominent mass-transport deposits are seen in the top ~500 meters (~1600 ft) of the subsurface and are characterized by low to moderate amplitude, discontinuous reflections. An inactive pockmark of 618 m (2030 ft) diameter is also found in the Choctaw Basin, indicating a previous gas expulsion event.

The BSR is a notable feature in the Choctaw syncline that cross-cuts the dipping stratigraphic reflections. The BSR has a reversed polarity from the seafloor, signifying the increased impedance traversing from hydrate to free gas in sediment pore space (Holbrook et al., 1996). Pore-filling hydrate may act as a seal that prevents the upward migration of gas, and bright amplitudes terminating against the BSR in the syncline reflect this occurrence. Additionally, the discontinuous nature of the BSR is indicative of lithological variations, an expected result in a channelized basin (Hillman et al., 2017; Shedd et al., 2012; Birchwood et al., 2010).

Very high amplitude reflections occur on the western flank of the Choctaw Basin. Several channel systems cross this flank, and the bright amplitudes may be attributed to

the impedance contrast between coarse-grained channel sands and surrounding muds. Higher amplitudes along this structural high may also be caused by a small amount of gas in the pore space, as the presence of gas hydrate implies some free gas is present below the BSR.

After mapping was completed, the seismic data was broken into two broad sections based on reflection character and interpreted channel presence. The top section, **Unit 1**, is dominated by strong to moderate amplitude, continuous reflections. This interval shows a transition from turbidite channels to slump features as the dominant flow mechanism. The lower **Unit 2** extends from the base of Unit 1 to the top of salt and is characterized by semi-continuous reflections of variable amplitude. The difference in seismic character from Unit 1 is attributed to the numerous turbidite channels present throughout this section. **Figure 4** shows an illustrated interpretation of the line used in Figure 3, highlighting the notable seismic features.

Channel Systems in the Orca and Choctaw Basins

Thirty-five channel systems were mapped in the study area to analyze morphological trends and variations. In general, channels in the Orca and Choctaw basins have low relief and are not easily distinguished in profile-view alone. The average channel height of the mapped systems was 57 m (187 ft), with a maximum observed height of 100 m (329 ft). Channel width averaged 620 m (2034 ft) but spanned a wide range, with narrowest channels measuring ~250 m (820 ft) and the largest channel measuring 1260 m (4134 ft). See **Table 1** for a summary of mapped channel attributes.

Channel systems identified in profile generally appear as either amplitude bright spots that lack an incised base, or as incised-base systems with low or variable amplitude fill. Channels may have erosional and/or depositional characteristics (Normark et al., 1993; Mutti and Normark, 1991), and this interpretation is used to categorize the morphologies observed in the study area. In this case, channels with high amplitude fill that lack an incised base are interpreted to be deposition-dominated and categorized as **Type 1**, while channels with an incised base and low or variable amplitude fill are interpreted to be erosional or mixed erosional-depositional systems and classified as **Type 2 (Fig. 5)**. Of the thirty-five channels mapped, only three were classified as

deposition-dominated; most channels showed some combination of both processes and were therefore classified as Type 2.

Levees are not easily distinguished in the seismic data. When visible, levees are associated with Type 2 channels only. While the channel systems have low relief and accompanying levees may be below the resolution of the seismic data, lack of levees can also be indicative of more distal channel systems (McHargue et al., 2010; Posamentier and Kolla, 2003; Kane et al., 2010). In the few cases where levees are present, the characteristic wedge-shaped deposits are nearly transparent in profile, with faint leading seismic troughs **(Fig. 6)**. These troughs are likely indicative of the thinly-bedded sands that have been documented in some levee deposits (Posamentier and Kolla, 2003; Clemenceau et al., 2000; Normark et al., 1993). In comparing channels with levees to those without, a higher magnitude discharge and more sustained flow are attributed to the former, allowing for greater overbanking of sediment and longer periods of deposition for levees to aggrade.

Channel sinuosity was highly variable in the study area. Most channels mapped have low sinuosity, but in several systems the sinuosity was very high **(Table 1)**. Multiple factors can impact this attribute, including gradient, seafloor topography, and the magnitude of the flow versus the channel's degree of confinement (Clark et al., 1992; Clark and Pickering, 1996; Mayall and Casey, 2006; Kane et al., 2008). In this case, sinuosity was not correlative to variables such as channel width or depth, but Type 1 depositional channels all appear to have low sinuosity. Type 2 channels, on the other hand, show a range of sinuosity patterns, and Mayall et al., 2006, listed an initial erosive

base as a cause of sinuosity in turbidite channels. Additionally, all channels with high sinuosity were deposited relatively early (before deposition of Hrz005), suggesting basin morphology may also play a role in sinuosity. Examples of varying degrees of sinuosity observed in the study area are shown in **Figure 7.**

The primary goal of this research was to identify where coarse-grained sediments that could serve as hydrocarbon reservoirs are found in the basin. In seismic data, high amplitude reflections associated with channels are often interpreted to be sand-rich (Posamentier and Kolla, 2003). In the Orca and Choctaw basins, where these high amplitude reflections occur largely corresponds to interpreted channel type. Type 1 deposition-dominated systems appear as high amplitude, single channel 'blips' in profile, with bright amplitudes largely confined to the channel axis in plan view **(Fig. 5a)**. In addition, these blips often have a slight thickness anomaly compared to adjacent reflections, interpreted to be the differential compaction of sandier channel fill surrounded by fine-gained muds (Hadler-Jacobsen, 2005).

Type 2 channels often have a brighter, seismically negative base in profile indicating coarser sediment lag. Channel fill may be predominately low-amplitude, indicating a channel filled with muds (Mayall et al., 2006), or a mix of low and high amplitude reflections that indicates a mix of coarse and fine-grained lithologies. In the case of the latter, higher amplitudes interpreted as sands often appear along the channel wall, especially in sinuous channels where increased deposition at channel bends is anticipated (McHargue et al., 2010; Clark and Pickering, 1996; Kane et al., 2008) **(Fig.**

5b). Increased sinuosity also corresponds to brighter amplitudes found outside the channel margins, interpreted here as the overbanking of fine-grained sands **(Fig. 7e)**.

In broad, low-sinuosity Type 2 channels, bright amplitude occurrence can become quite complex. In one mapped system, bright amplitudes have a patchier distribution reflecting a complex internal channel morphology. This high amplitude distribution likely corresponds to preferential sand deposition at internal channel benches, as described in Clark and Pickering (1992) **(Fig 8).**

A notable distributary channel system also occurs in the dataset. A majority of the channels in the dataset appear as single channels with a general northwest-southeast flow direction, but a large west-east trending system also crosses the southern portion of the study area. This system terminates in a well-developed fan in the Choctaw syncline **(Fig. 9**). Such fans are often associated with sheet sands (Posamentier and Kolla, 2003), likely contributing to the high amplitudes in the syncline interpreted as coarse-grained sediments.

Well Log Interpretation

Four industry appraisal wells were drilled in the study area by Unocal/Chevron between 2011 and 2013. One of these wells, WR143-002, was plugged and abandoned shortly into drilling after casing became stuck in the wellhead, therefore only the remaining three wells are incorporated into this research. Available logs include gamma ray and a suite of resistivity logs for each of the three wells WR98-001, WR143-001, and WR143-003. Sonic logs were also available for the WR143- wells. Caliper and density logs over the shallow (<4500 mbsl) area of interest were not collected for the wells and are therefore not included in the interpretation.

The wells are concentrated on the western side of the seismic dataset, on or near the salt-cored anticline that forms the western flank of the Choctaw syncline. Correlating between wells using the gamma ray and resistivity curves alone is challenging due to normal faulting across the anticline and varying proximity to channel margins. However, projecting the wells onto the largely continuous reflections in the seismic data allows correlations to be made with a reasonable degree of confidence.

In general, all three wells are dominated by fine-grained muds and silts, with varying degrees of interbedded sands. Coarsening upwards sequences indicating sea level rise and fall are identifiable in all three gamma ray logs. Resistivity logs indicate

water-filled pores in the majority of sediments, with several high resistivity spikes associated with gas hydrate. Detailed interpretations for each well follow.

WR98-001 ***(Fig. 10)***

WR98-001 is located on the western side of the study area between the Orca and Choctaw basins. The mudline depth was not included in the available well data, but the depth-migrated seismic data shows the seafloor at 1858 mbsl (6096 fbsl). The well was drilled to a total measured depth of 9688 mbsl (31784 fbsl), penetrating the top of salt at 3740 mbsl (12270 fbsl).

Where most sands in all three wells occur as heavily interbedded stringers, WR98-001 is notable for having a thick, relatively clean wet sand from 2099-2133 mbsl (6887-7000 fbsl). The interpreted lithology and fluid fill is based on low gamma ray and resistivity readings, signifying low clay content and more permeable, water-filled sediment. This interval corresponds to a seismic trough that was mapped from WR98-001. An instantaneous amplitude map of this horizon does not show any clear channel features in the well area; however heavy normal faulting may have obscured any linear trends **(Fig 11)**. The sand may also represent a splay coming in from the northwest, outside the range of the seismic data.

In addition to this clean sand, interbedded sand intervals more typically found in the well logs are present in WR98-001 from 2469-2616 mbsl (8101-8585 fbsl), 2712-2836 mbsl (8898-9304 fbsl), and 3131-3448 mbsl (10273-11312 fbsl). A cleaner,

isolated sand also occurs from 2976-2981 mbsl (9765-9781 fbsl) based on low gamma ray levels and a sharp decrease in resistivity.

WR143-003 ***(Fig. 12)***

Well WR143-003 is located along the western side of the western ridge of the Choctaw Basin, 1890 meters (6200 feet) southeast of WR98-001. The recorded water depth at the well is 1757 meters (5764 feet), and it was drilled to a total measured depth of 8637 mbsl (28,338 fbsl). The salt canopy was encountered at 3472 mbsl (11,392 fbsl). The most notable feature in the WR143-003 logs is a prominent resistivity spike from 2116 to 2179 mbsl (6943-7149 fbsl). This spike is located above an inferred BSR of 2237 mbsl (7342 fbsl) and is likely caused by gas hydrate. Low to moderate gamma ray readings in the bottom half of the interval indicate a pore-filling hydrate morphology, while higher gamma ray counts in the upper half leads to the interpretation of gas hydrate in fractures.

Below the hydrate, low gamma readings throughout the log indicate frequent interbedded sands. Corresponding drops in the resistivity log indicate particularly permeable intervals between 2555-2703 mbsl (8382-8867 fbsl), 2843-3088 mbsl (9328-10132 fbsl), 3193-3243 mbsl (10476-10640 fbsl), and 3277-3331 mbsl (10750-10929 fbsl).

WR143-001 ***(Fig. 13)***

WR143-001 is located on eastern side of the western Orca-Choctaw Basin ridge, 2506 m (764 ft) east of WR143-003. The well was drilled in 1683 m (5523 ft) of water to a measured depth of 3665 mbsl (12,023 fbsl). Salt was not penetrated at this location due to drilling difficulties that caused the well to be abandoned before reaching the target depth. A shallow water flow zone was also noted in the drilling report at 2434 mbsl (7984 fbsl).

The WR143-001 well logs shows two shallow resistivity spikes from 1864-1885 mbsl (6115-6185 fbsl) and 1980-2002 mbsl (6497-6568 fbsl). The gamma ray in each of these cases indicates a relatively impermeable lithology. In addition, these spikes are well above an inferred base of hydrate stability at 2189 mbsl (7183 fbsl), and are therefore interpreted to be gas hydrate in fractures.

In general, WR143-001 has higher gamma ray levels than WR98-001 and WR143-003, indicating an overall muddier lithology. Some sands are still present, however, as indicated by coincident drops in the gamma ray and resistivity logs. The most prominent of these sand sections is a wet, interbedded interval from 2882-2945 mbsl (9456-9663 fbsl), located immediately below a casing point at 2880 mbsl (9450 fbsl). More permeable intervals are also indicated from 2181-2220 mbsl (7158-7283 fbsl), 2357-2434 mbsl (7734-7984 fbsl), and 2520-2669 mbsl (8269-8755 fbsl).

Well Lithology and Channel Proximity

The coarsest turbidity flow sediments are generally found within the channel (Mutti and Normark, 1991). In this case, none of the wells appear to directly penetrate a

channel **(Fig. 14)**, and the more permeable intervals listed above are interpreted as thinly interbedded overbank deposits. This interpretation is supported by a generally positive correlation between sand content in the well log and channel proximity. **Figures 10, 12**, and **13** identify nearby mapped channel systems that correspond to sandier intervals on the logs.

More permeable intervals not linked to a mapped channel system may still have some turbidite involvement. Many of the channels identified in the study area are small, single channel systems; others may exist that are below the resolution of the seismic data. Some sands may also represent unconfined flow deposits, such as fans or sheets. It is also very likely that additional channels are present near the wells that are obscured by faults, the BSR, and/or a small amount of gas in sediment pore-space. Since all these features are interpreted to occur along the western flank of the Choctaw Basin, and are therefore proximal to the wells, some channel obscurement is likely.

Depositional Trends

Basin morphology plays a key role in channel morphology and occurrence, in turn influencing where coarse-grained sediments are ultimately deposited. Salt withdrawal is progressive and changes the shape of a basin over time; understanding the timing of uplift is therefore an important part of the channel story. Further, the progressive salt withdrawal that formed the Orca and Choctaw minibasins was not isolated to the study area, and different rates of uplift on modern basin ridges are entirely possible.

Flattening on mapped horizons shows the modern Choctaw syncline was largely flat-lying in the west-east direction when most of the mapped channels were deposited. The deepest interval, flattened on Hrz005 and highlighted down to Hrz001, shows some thinning to the western extent of the dataset, with maximum accommodation located on the western side of the modern syncline **(Fig. 15a)**. Flattening on Hrz100 and Hrz400 shows slight thinning over the western ridge and maximum accommodation shifting eastward **(Fig. 15b-c)**. While this indicates some uplift was occurring, dip estimations for the western ridge when Hrz400 was deposited are still less than 1°. The channels shown in **Figure 7b** were deposited during this time, demonstrating that uplift was still minor enough to allow channels to cross the western ridge.

Flattening on Hrz500 shows enhanced thinning on the western ridge along with strong uplift of the eastern ridge. The eastern uplift is interpreted to occur at least partially in response to the increased loading on the eastern side of syncline; this uplift in turn shifted maximum accommodation back towards the center of the basin **(Fig. 15d)**. In the final two intervals, flattening on horizons Hrz750 and the seafloor show continued uplift of the modern ridges and maximum subsidence shifting into the center of the modern syncline **(Fig 15e-f)**.

Subtle variations in isopachs between the mapped horizons corroborate the early shift of maximum accommodation from the western to eastern side of the modern Choctaw syncline **(Fig. 16a-c)**, with late uplift of the eastern flank eventually shifting maximum accommodation back to the center of the basin **(Fig. 16d-e)**. The uplift of the northern ridge that separates the Orca and Choctaw basins can also be seen in the isopachs, with maximum accommodation shifting from the northern to southern portion of the modern syncline. The steeper basin gradient in **Figure 16e** shows maximum uplift rates occurred after Hrz400 was deposited, in turn impacting the type of gravity flow occurring in the basin. While turbidite channels were prevalent in the deeper intervals classified as seismic Unit 2, slump features dominate in the shallower Unit 1 intervals **(Figure 16f)**.

Discussion

The Orca and Choctaw basins show evolving depositional trends shaped by progressive salt withdrawal. Well logs show a lithology dominated by muds and silts with thinly interbedded sands. Sand content generally increases with proximity to a channel system, and this relationship can be used to predict coarse-grained sediment occurrence in study areas with poor well control.

Channel systems occur in a range of morphologies but can be broadly classified by their erosive and depositional elements. Higher sinuosity was observed in Type 2 channels with an erosive element, although low-sinuosity variations were also observed. Basin gradient may play a role in this attribute, as channels with higher sinuosity were identified only in deeper intervals when the basin was comparatively flat-lying. Gradient is clearly not the only control, however, as low sinuosity channels are also found in deeper intervals. Factors such as discharge magnitude and the confining capacity of the channel have been experimentally shown to impact sinuosity in submarine channels (Kane et al., 2008), and a correlation between coarser bedloads and low sinuosity has also been suggested (Clark et al., 1992). Type 1 channels may reflect this latter relationship, as the bright amplitude channel fill interpreted as sand-rich also corresponds to low planform sinuosity.

The evolving shape of the basin also impacts channel directionality and occurrence. Twenty-four of the thirty-five channels mapped have a northwest-southeast flow direction, but a well-defined west-east trending distributary system also deposits sediments into the Choctaw Basin. An early structural high to the west of the dataset is indicated by flattening on the deeper horizons **(Fig. 15a)**, and the extensive west-east trending system likely originates from this area and provides a second source of sediment to the Choctaw syncline. In addition, displaying all channels mapped in profile shows the deepest channel systems were concentrated on the western side of the modern Choctaw syncline, exploiting the early topographic low. This concentration shifts eastward in subsequent systems, as northwest-southeast trending channels follow the migrating depocenter caused by uplift of the western ridge. **(Fig. 14)**.

Plotting the well logs alongside an extracted seismic trace from each well site allows the two data types to be integrated. As expected, higher amplitude seismic reflections in the dataset often correspond to low gamma ray counts indicating sands (**Figures 10, 12, and 13)**, particularly in thin, isolated sands where the acoustic impedance changes rapidly from mud to sand and back to mud. Caution should be used in interpreting sediments based on seismic character alone, however, particularly in areas with poor well control. Thick, homogenous sands can have low internal impedance contrast, and the resulting low amplitude reflections may be misinterpreted as muds (Mayall et al., 2006). As an example, the more sand-dominated interval from 2882-2945 mbsl (9456-9663 fbsl) in WR143-001 corresponds to relatively low amplitudes in the seismic trace **(Figure 13).**

As turbidite channels are the primary conduits of coarser, terrestrially-sourced sediments on the outer Gulf of Mexico shelf, interpreting lithology based on proximity to channel margins can help counteract some of the ambiguity inherent to seismic reflections. Post-depositional processes may also help distinguish thick sand intervals from muds. For example, differential compaction of sands and muds will often create a thickness anomaly in the sands; larger channels may appear to have a mounded top over the channel axis due to the comparatively lower compressibility of sands. **Figure 17** is an example of mounding over the channel axis, indicating a more sand-rich channel fill.

Geophysical indicators may also help to identify coarser-grained lithologies when channel features are obscured. Gas hydrate causes acoustic impedance to increase, often resulting in a leading peak in seismic data (McConnell et al., 2012). This relationship is seen in **Figure 13**, where the top of the gas hydrate interval interpreted as hydrate in fractures corresponds to a moderate amplitude seismic peak. A much stronger leading peak occurs over the BSR to the eastern side of the dataset, where channels features cannot be mapped due to an overlying mass transport deposit and the eastern extent of the dataset **(Figure 4).** The stronger geophysical response in this area could result from a coarser-grained lithology in which hydrate occurs as sediment pore-fill, rather than being confined to fractures.

Summary

The related processes of sediment supply and salt withdrawal resulted in the basins we see today. Sediments largely sourced from the northern coastline are carried into the study area by turbidite channels, creating load that causes salt to withdraw. The salt migrates to areas of decreased load along the flanks, creating salt-cored anticlines that enhance adjacent accommodation space. Channels flow into the area of maximum accommodation and deposit sediments within the channel axis and as levee and overbank deposits. These sediments fill accommodation, increase load, and cause more salt to withdraw.

Prediction of coarse-grained sediment occurrence through channel identification and seismic-well log integration is a key step in identifying potential reservoirs for hydrocarbons. In salt withdrawal mini-basins, evolving basin shape impacts channel morphology and occurrence, influencing where coarse-grained sediments are ultimately deposited. In this study, thirty-five channel systems were mapped using seismic profiles and amplitude analysis. Morphological characteristics of these channels were categorized to predict where amplitude bright spots corresponding to sands are most likely to occur, and flattened horizons and isopachs allow variations in channel

morphology to be placed in the context of overall basin development. Well logs were also used to show the correlation between sand content and channel proximity.

This study provides a detailed assessment of the channel systems in the study area, as well as a comprehensive sedimentological interpretation of the basins post-salt deposition. In addition to identifying potential coarse-grained reservoirs within the Orca and Choctaw basins, this research serves as a model for other studies using seismic and well log data to interpret turbidite channels in deepwater basins.

References

Addy, S. K., & Behrens, E. W. (1980). Time of accumulation of hypersaline anoxic brine in Orca basin (Gulf of Mexico). *Marine Geology*, *37*(3–4), 241–252. http://doi.org/10.1016/0025-3227(80)90104-8

Alexander, L. L., Flemings, P. B. (1995). Geologic Evolution of a Pliocene-Pleistocene Salt-Withdrawal Minibasin: Eugene Island Block 330, Offshore Louisiana. *AAPG Bulletin, 79*. doi:10.1306/7834deea-1721-11d7-8645000102c1865d

Bahorich, M. B., Farmer, S. L. (1996). 3-D Seismic Discontinuity for Faults and Stratigraphic Features: The Coherence Cube: ABSTRACT. *AAPG Bulletin, 80*. doi:10.1306/64ed894e-1724-11d7-8645000102c1865d

Birchwood, R., Shelander, D., Boswell, R., Virginia, W., Collett, T., Cook, A., & Murray, D. (2010). Developments in Gas Hydrates. *Oilfieild Review, Spring 201*, 18–33.

Boswell, R. and Collett, T.S. (2010) Current perspectives on gas hydrate resources, *Energy and Environmental Science.* DOI: 10.1039/c0ee00203h.

Chopra, S., & Marfurt, K. J. (2012). Seismic attribute expression of differential compaction. *SEG Technical Program Expanded Abstracts 2012*. doi:10.1190/segam2012-1323.1

Clark, J. D., Kenyon, N. H., & Pickering, K. T. (1992). Quantitative analysis of the geometry of submarine channels: Implications for the classification of submarine fans. *Geology*, *20*(7), 633. doi:10.1130/0091-7613(1992)020<0633:qaotgo>2.3.co;2

Clark, J. D., & Pickering, K. T. (1996). Architectural elements and growth patterns of submarine channels: Application to hydrocarbon exploration. *AAPG Bulletin*. http://doi.org/10.1306/64ED878C-1724-11D7-8645000102C1865D

Clemenceau, G. R., Colbert, J., & Edens, D. (2000). Production Results from Levee-Overbank Turbidite Sands at Ram/Powell Field, Deepwater Gulf of Mexico. *Deep-Water Reservoirs of the World: 20th Annual*, 241-251. doi:10.5724/gcs.00.15.0241

Clennell, M. B., Hovland, M., Booth, J. S., Henry, P., & Winters, W. J. (1999). Formation of natural gas hydrates in marine sediments: 1. Conceptual model of gas hydrate growth conditioned by host sediment properties. *J. Geophys. Res. Journal of Geophysical Research: Solid Earth, 104*(B10), 22985-23003. doi:10.1029/1999jb900175

DSDP 96 Part I, Chapter 17: Site 618. http://doi:10.2973/dsdp.proc.96.117.1986

Hadler-Jacobsen, F., Johannessen, E. P., Ashton, N., Henriksen, S., Johnson, S. D., & Kristensen, J. B. (2005). Submarine fan morphology and lithology distribution: a predictable function of sediment delivery, gross shelf-to-basin relief, slope gradient and basin topography. *Petroleum Geology: North-West Europe and Global Perspectives – Proceedings of the 6th Petroleum Geology Conference*,1121-1145. doi:10.1144/0061121

Hillman, J. I. T., Cook, A. E., Sawyer, D. E., Küçük, H. M., & Goldberg, D. S. (2017). The character and amplitude of "discontinuous" bottom-simulating reflections in marine seismic data. *Earth and Planetary Science Letters*, *459*, 157–169. http://doi.org/10.1016/j.epsl.2016.10.058

Holbrook, W. S., Hoskins, H., Wood, W. T., Stephen, R. A., Lizarralde, D., & Party, L. 1. (1996). Methane Hydrate and Free Gas on the Blake Ridge from Vertical Seismic Profiling. Science, 273(5283), 1840-1843. doi:10.1126/science.273.5283.1840

Hubbard, S. M., Covault, J. A., Fildani, A., & Romans, B. W. (2014). Sediment transfer and deposition in slope channels: Deciphering the record of enigmatic deep-sea processes from outcrop. *Geological Society of America Bulletin, 126*(5-6), 857-871. doi:10.1130/b30996.1

Jiang, S., Weimer, P., Henriksen, S., & Hammon, W. S. (2012). 3D Seismic Stratigraphy and Evolution of Upper Pleistocene Deepwater Depositional Systems, Alaminos Canyon, Northwestern Deep Gulf of Mexico. *Application of the Principles of Seismic Geomorphology to Continental-Slope and Base-of-Slope Systems: Case Studies from Seafloor and Near-Seafloor Analogues*, 309-327. doi:10.2110/pec.12.99.0309

Kane, I. A., Mccaffrey, W. D., & Peakall, J. (2008). Controls on sinuosity evolution within submarine channels. *Geology, 36*(4), 287. doi:10.1130/g24588a.1

Kane, I. A., McCaffrey, W. D., Peakall, J., & Kneller, B. C. (2010). Submarine channel levee shape and sediment waves from physical experiments. *Sedimentary Geology*. http://doi.org/10.1016/j.sedgeo.2009.11.001

Bureau of Ocean Energy Management. Klazynski, R., Klocek, E., Nixon, L., Petty, A., Post, P. (2012). Assessment of Technically Recoverable Hydrocarbon Resources of the Gulf of Mexico Outer Continental Shelf as of January 1, 2009. https://www.boem.gov/GoM-2011-National-Assessment/

Kou, W. W.-H., Smith, M. A., Ahmed, A., & Kuzela, R. (2007). Direct seismic indicators of gas hydrates in the Walker Ridge and Green Canyon areas, deepwater Gulf of Mexico. *The Leading Edge*, *26*(2), 152–155. http://doi.org/10.1190/1.2542440

Kvenvolden, K. A. (1993). Gas hydrates-geological perspective and global change. *Reviews of Geophysics, 31*(2), 173-187. doi:10.1029/93rg00268

Madof, A. S., Christie-Blick, N., & Anders, M. H. (2009). Stratigraphie controls on a salt-withdrawal intraslope minibasin, north-central Green Canyon, Gulf of Mexico: Implications for misinterpreting sea level change. *AAPG Bulletin*. http://doi.org/10.1306/12220808082

Malinverno, A. (2010). Marine gas hydrates in thin sand layers that soak up microbial methane. *Earth and Planetary Science Letters*, *292*(3–4), 399–408. http://doi.org/10.1016/j.epsl.2010.02.008

Marfurt, K. J., Kirlin, R. L., Farmer, S. L., & Bahorich, M. S. (1998). Coherency Algorithm. *Geophysics*, *63*(4), 1150–1165.

Mayall, M., Jones, E., & Casey, M. (2006). Turbidite channel reservoirs-Key elements in facies prediction and effective development. *Marine and Petroleum Geology*. http://doi.org/10.1016/j.marpetgeo.2006.08.001

Mcconnell, D. R., & Kendall, B. A. (2003). Images of the base of gas hydrate stability in the deepwater Gulf of Mexico: Examples of gas hydrate traps in northwest Walker Ridge and implications for successful well planning. *The Leading Edge, 22*(4), 361-367. doi:10.1190/1.1572091

McConnell, D. R., Zhang, Z., & Boswell, R. (2012). Review of progress in evaluating gas hydrate drilling hazards. *Marine and Petroleum Geology*. http://doi.org/10.1016/j.marpetgeo.2012.02.010

Mchargue, T., Pyrcz, M., Sullivan, M., Clark, J., Fildani, A., Romans, B., Covault, J., Levy, M., Posamentier, H., Drinkwater, N. (2011). Architecture of turbidite channel systems on the continental slope: Patterns and predictions. *Marine and Petroleum Geology, 28*(3), 728-743. doi:10.1016/j.marpetgeo.2010.07.008

Mutti, E., & Normark, W. R. (1991). An Integrated Approach to the Study of Turbidite Systems. *Frontiers in Sedimentary Geology Seismic Facies and Sedimentary*

Processes of Submarine Fans and Turbidite Systems, 75-106. doi:10.1007/978-1-4684-8276-8_4

Normark, W. R., Posamentier, H., & Mutti, E. (1993). Turbidite systems: State of the art and future directions. *Reviews of Geophysics, 31*(2), 91-116. doi:10.1029/93rg02832

Pilcher, R. S., & Blumstein, R. D. (2007). Brine volume and salt dissolution rates in Orca Basin, northeast Gulf of Mexico. *AAPG Bulletin*, *91*(6), 823–833. http://doi.org/10.1306/12180606049

Posamentier, H. W., Davies, R. J., Cartwright, J. A., & Wood, L. (2007). Seismic geomorphology - an overview. *Geological Society, London, Special Publications,277*(1), 1-14. doi:10.1144/gsl.sp.2007.277.01.01

Posamentier, H. W., & Kolla, V. (2003). Seismic Geomorphology and Stratigraphy of Depositional Elements in Deep-Water Settings. *Journal of Sedimentary Research, 73*(3), 367-388. doi:10.1306/111302730367

Shedd, W., Boswell, R., Frye, M., Godfriaux, P., & Kramer, K. (2012). Occurrence and nature of "bottom simulating reflectors" in the northern Gulf of Mexico. *Marine and Petroleum Geology*. http://doi.org/10.1016/j.marpetgeo.2011.08.005

Shokes, R. F., Trabant, P. K., Presley, B. J., & Reid, D. F. (1977). Anoxic, Hypersaline Basin in the Northern Gulf of Mexico. *Science, 196*(4297), 1443-1446. doi:10.1126/science.196.4297.1443

Sloan, E. D. (2003). Fundamental principles and applications of natural gas hydrates. *Nature, 426*(6964), 353-363. doi:10.1038/nature02135

Tompkins, R. E., & Shephard, L. E. (1979). Orca Basin: Depositional processes, geotechnical properties and clay mineralogy of Holocene sediments within an anoxic hypersaline basin, northwest Gulf of Mexico. *Marine Geology*, *33*(3–4), 221–238. http://doi.org/10.1016/0025-3227(79)90082-3

Trabant, P. K., & Presley, B. J. (1978). Orca Basin, anoxic depression on the continental slope, northwest Gulf of Mexico. *AAPG Studies in Geology*, *7*(1976), 303–311.

Tribovillard, N., Bout-Roumazeilles, V., Algeo, T., Lyons, T. W., Sionneau, T., Montero-Serrano, J. C, Riboulleau, A., Baudin, F. (2008). Paleodepositional conditions in the Orca Basin as inferred from organic matter and trace metal contents. *Marine Geology*, *254*(1–2), 62–72. http://doi.org/10.1016/j.margeo.2008.04.016

Weimer, P., & Link, M. H. (1991). Global Petroleum Occurrences in Submarine Fans and Turbidite Systems. *Frontiers in Sedimentary Geology Seismic Facies and*

Sedimentary Processes of Submarine Fans and Turbidite Systems, 9-67. doi:10.1007/978-1-4684-8276-8_2

Appendix: Table and Figures

Table 1. Mapped channel system attributes. Channels are numbered in ascending order from oldest to youngest.

Channel Name	Channel Height (ft)	Channel Height (m)	Channel Width (ft)	Channel Width (m)	Flow Direction	Sinuosity	Type 1 or 2
Channel 1	116	35	1444	440	NW-SE	Low	Type 2
Channel 2	228	69	1864	568	N-S	Moderate	Type 2
Channel 3	102	31	807	246	NW-SE	Moderate	Type 2
Channel 4	152	46	1585	483	NNE-SSW	High	Type 2
Channel 5	159	48	1224	373	NE-SW	High	Type 2
Channel 6	105	32	1184	361	NW-SE	Low	Type 1
Channel 7	211	64	2671	814	N-S	Low	Type 2
Channel 8	104	32	2139	652	NW-SE	High	Type 2
Channel 9	162	49	2146	654	NW-SE	Low	Type 2
Channel 10	64	20	1736	529	NNW-SSE	Very low	Type 1
Channel 11	144	44	3675	1120	NW-SE	Low	Type 2
Channel 12	286	87	2507	764	NW-SE	Low	Type 2
Channel 13	317	97	3563	1086	NE-SW	Low	Type 2
Channel 14	170	52	942	287	SW-NE	Low	Type 2
Channel 15	174	53	1404	428	NW-SE	Low	Type 1
Channel 16	233	71	2507	764	WNW-ESE	Moderate	Type 2
Channel 17	223	68	1916	584	W-E	Low to moderate	Type 2
Channel 18	275	84	4141	1262	NW-SE	Low	Type 2
Channel 19	460	140	2100	640	W-E	Low	Type 2
Channel 20	192	59	3757	1145	NW-SE	Moderate	Type 2
Channel 21	148	45	1181	360	NW-SE	Low	Type 2
Channel 22	102	31	1332	406	NW-SE	Low	Type 2
Channel 23	159	48	1670	509	NW-SE	Low	Type 2
Channel 24	117	36	2539	774	NW-SE	Low	Type 2
Channel 25	149	45	1568	478	WNW-ESE	Low	Type 2
Channel 26	286	87	1355	413	WNW-ESE	Low	Type 2
Channel 27	329	100	1319	402	WNW-ESE	low	Type 2
Channel 28	148	45	1391	424	NW-SE	Low	Type 2
Channel 29	202	62	2123	647	NNE-SSW	Low	Type 2
Channel 30	140	43	2159	658	NE-SW	Low	Type 2
Channel 31	150	46	3199	975	NE-SW	Low	Type 2
Channel 32	234	71	1916	584	NW-SE	Low	Type 2
Channel 33	191	58	2057	627	NW-SE	Low	Type 2
Channel 34	181	55	1808	551	NW-SE	Low	Type 2
Channel 35	138	42	2228	679	NW-SE	Low	Type 2

Figure 1. Regional maps of the Orca and Choctaw basins.

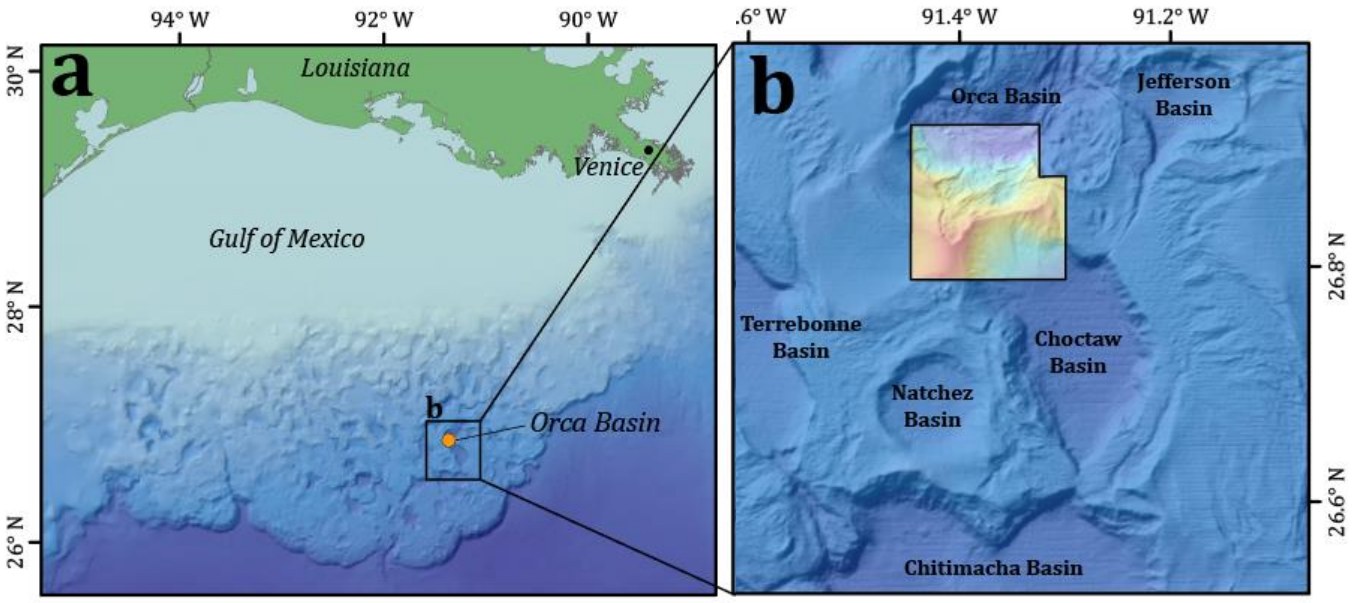

Figure 2. Seafloor map showing extent of 3-D seismic data (colored area) and industry well locations.

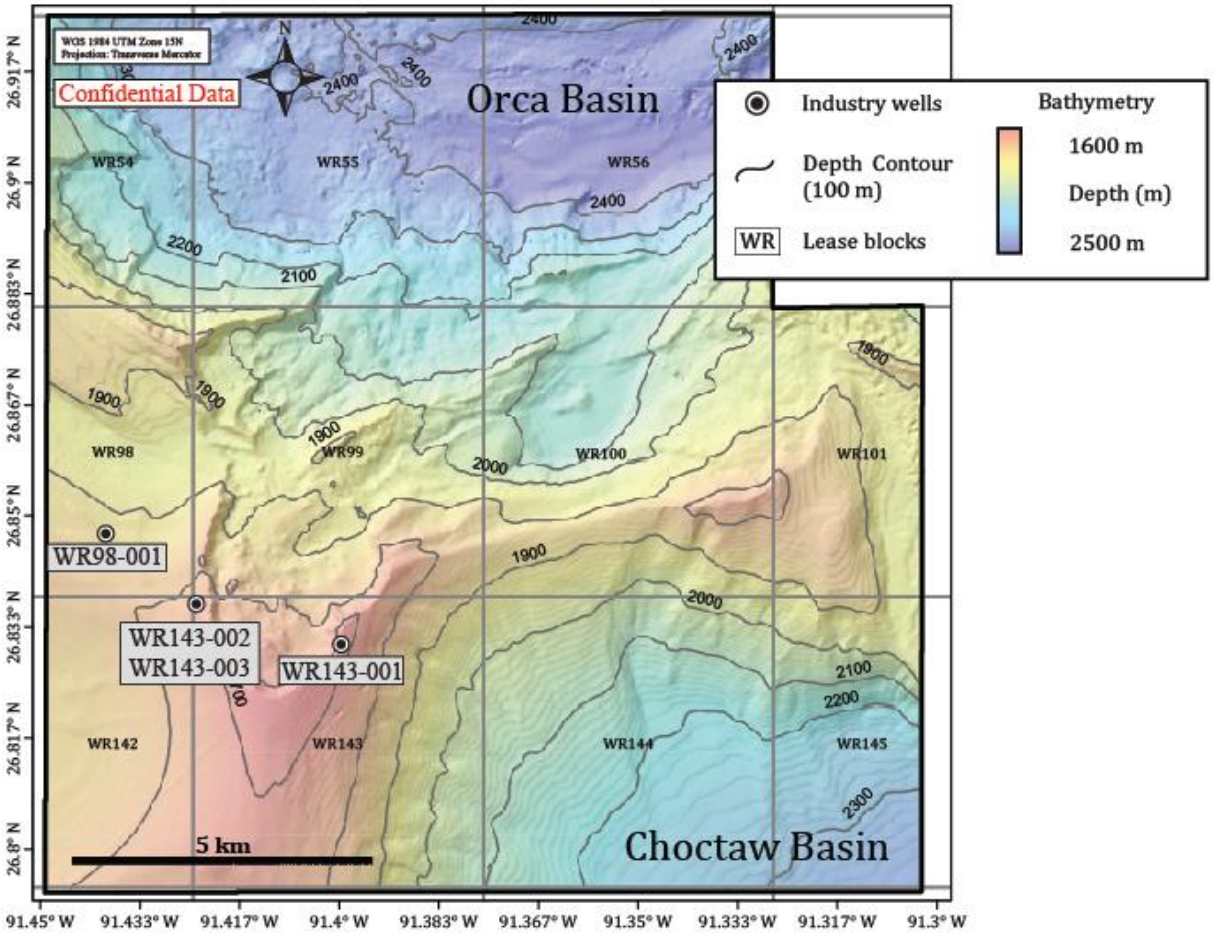

Figure 3. Arbitrary seismic line through industry wells showing all mapped horizons. Horizons are named in ascending order from oldest to youngest. Gamma ray and resistivity well logs are shown in green and red, respectively.

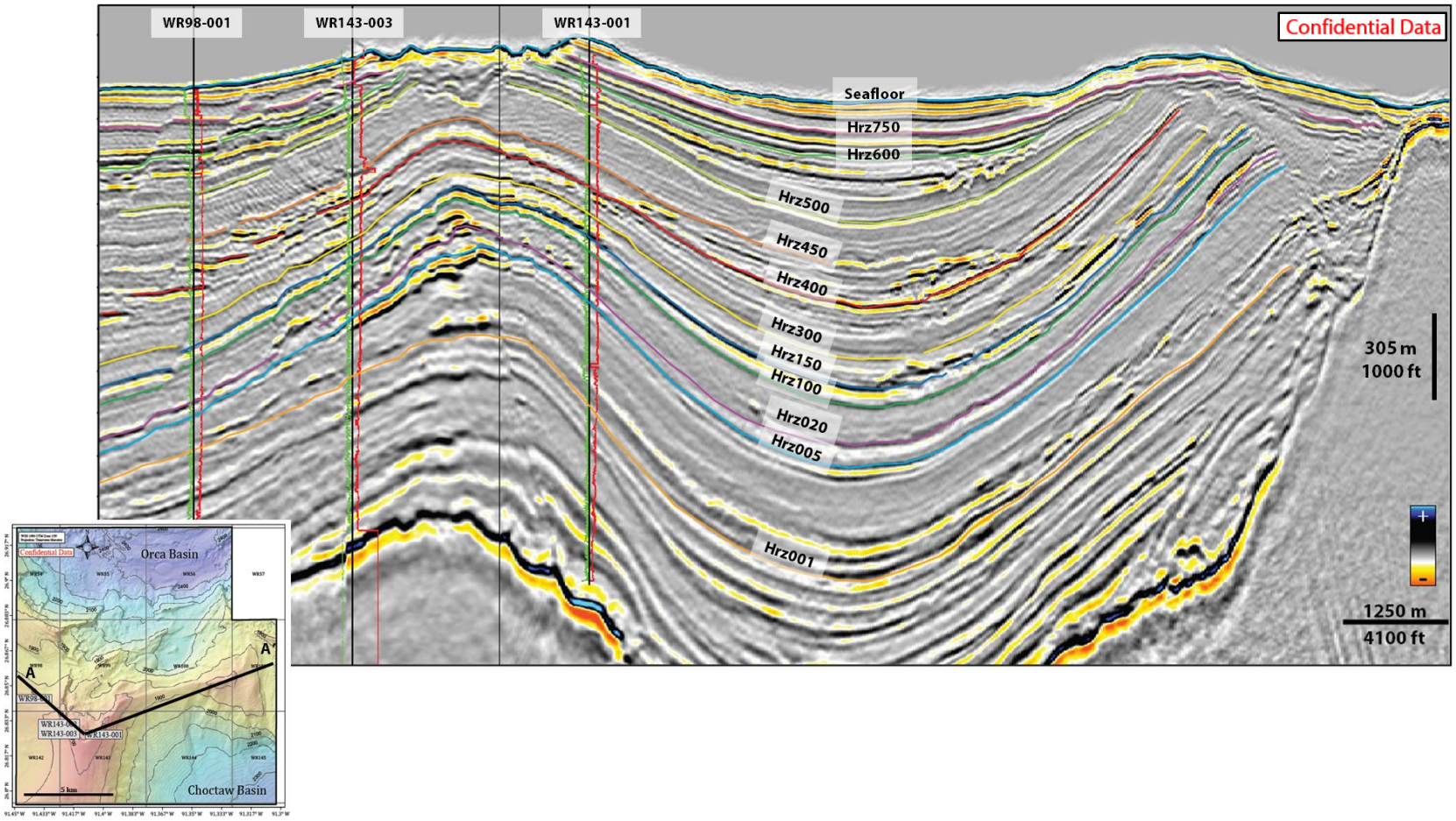

Figure 4. Illustrated interpretation of arbitrary line from Figure 3 showing select seismic features and mapped channel systems. Coarser-grained channel fill is indicated in yellow, while fining-outwards overbank deposits are shown in orange.

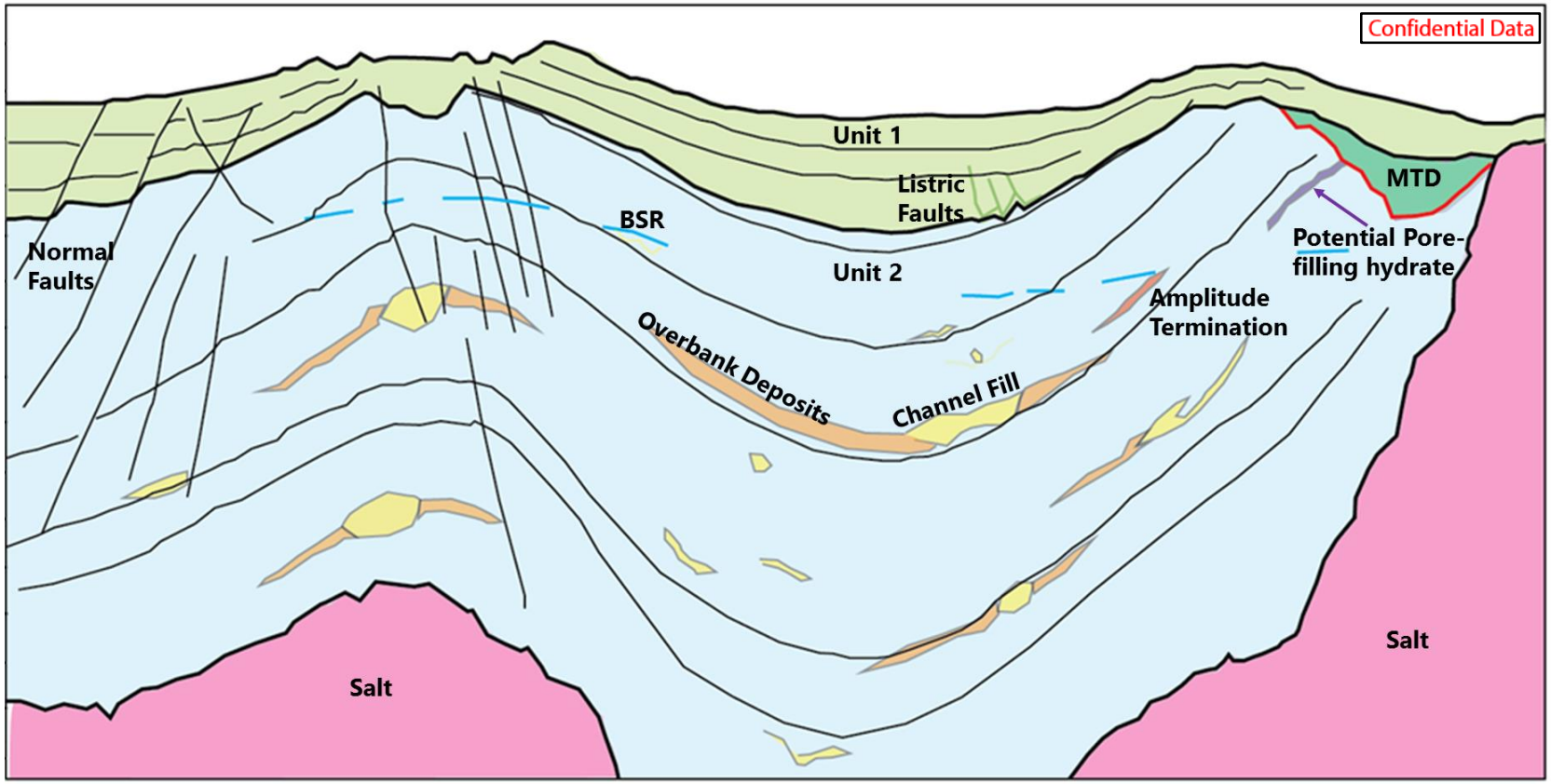

Figure 5. Basic channel morphologies. a) Type 1 channels lack an incised base in profile and show as well-constrained, low sinuosity amplitude anomalies in plan view. b) Type 2 channels have an incised base in profile and low to variable amplitude fill. Sinuous variations often show brighter amplitudes interpreted as sands along the channel wall.

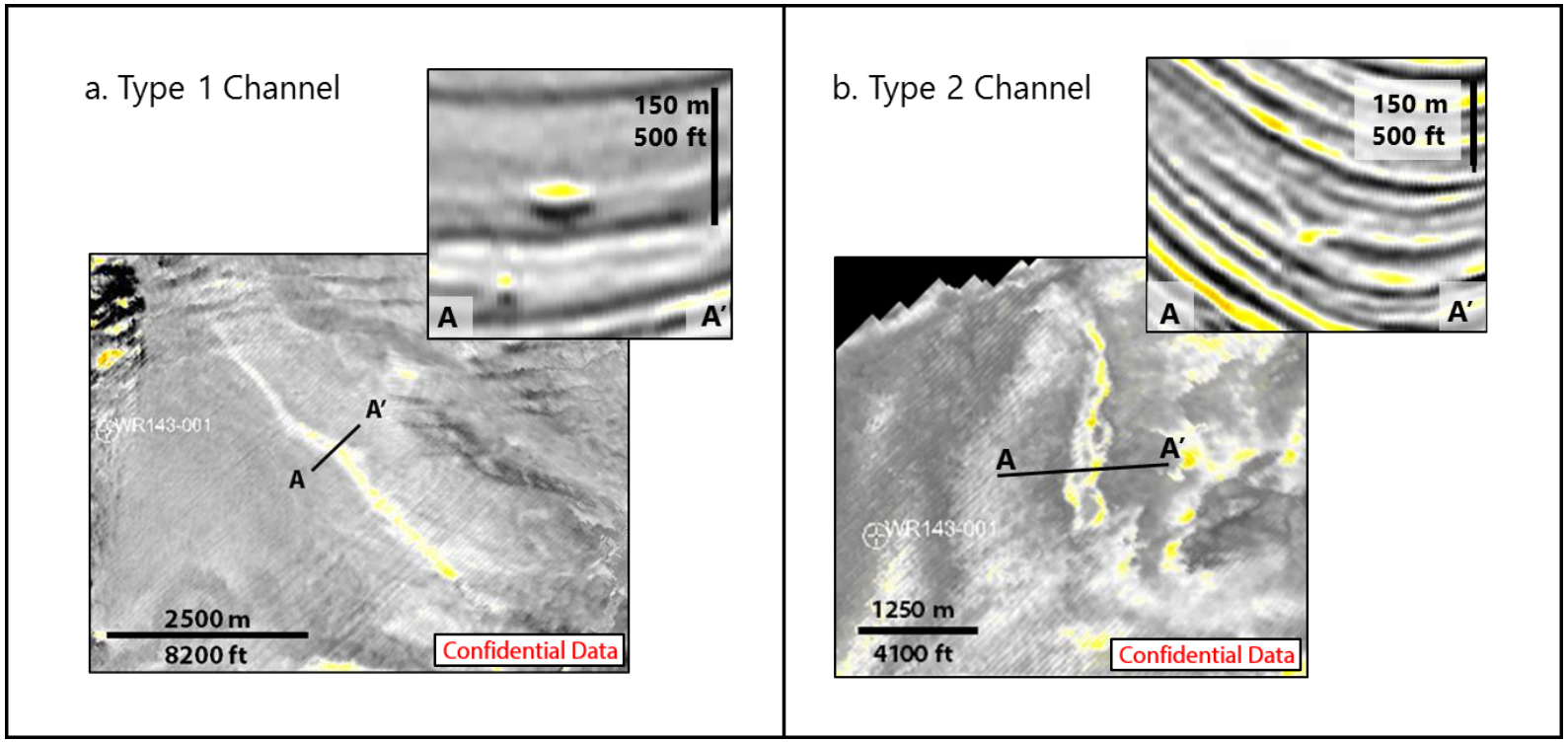

Figure 6. Channel levee in profile. Dashed red line shows interpreted base of channel.

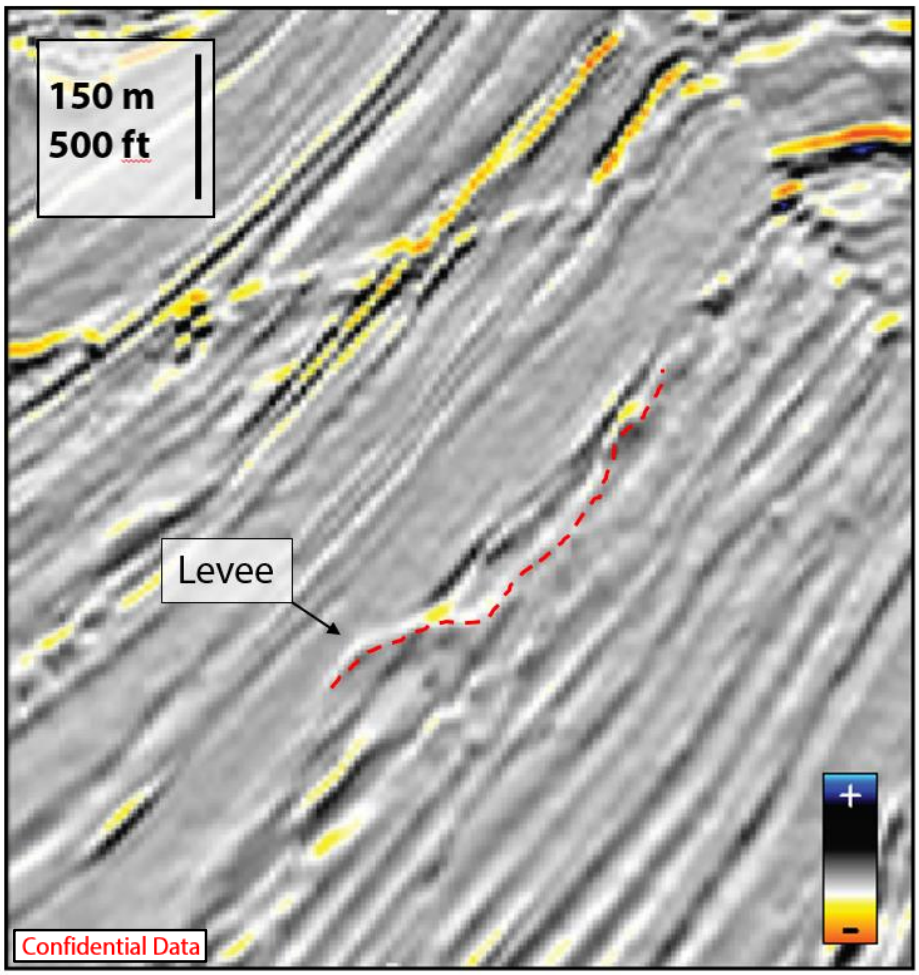

Figure 7. Amplitude maps showing sinuosity variations.

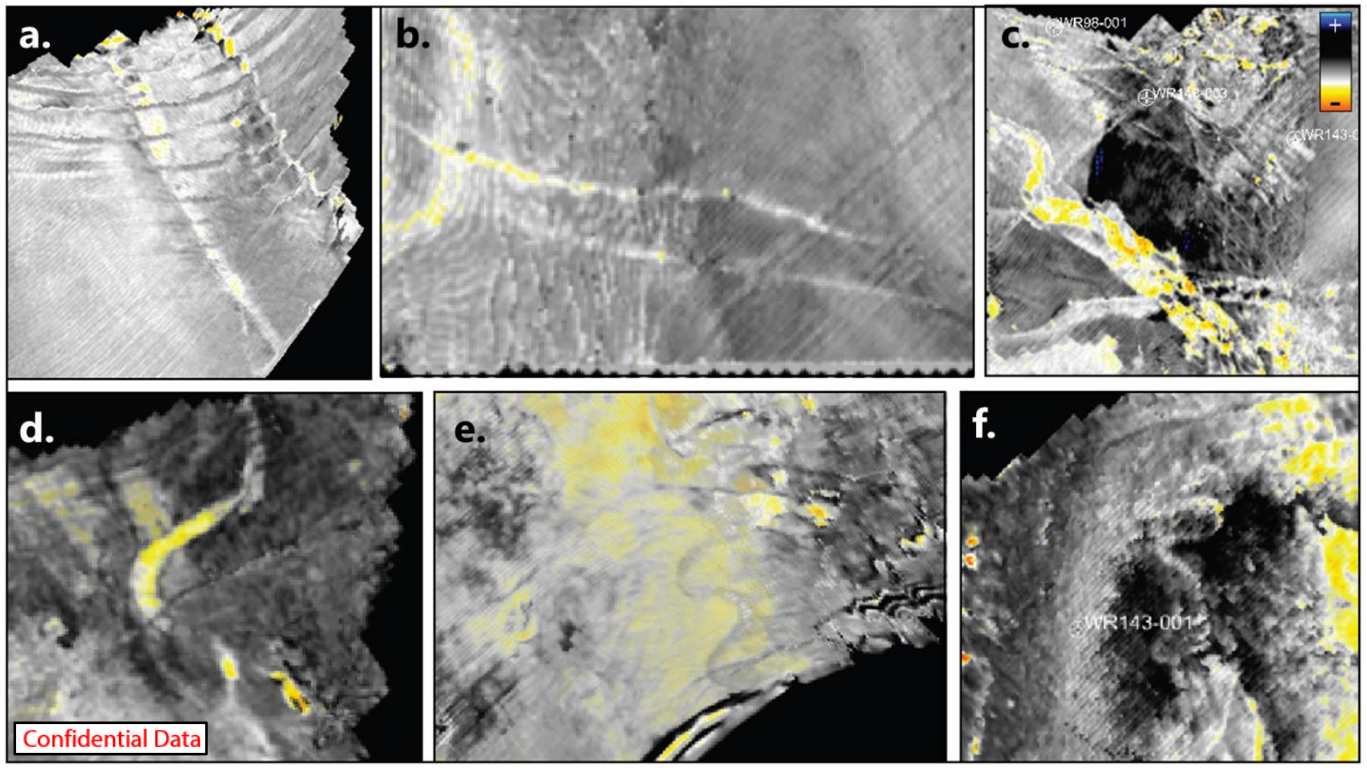

Figure 8. Low sinuosity channel complex. a) Interpretation of internal channel morphology, by Clark and Pickering, 1996. b) Amplitude map of channel in plan view showing bright amplitudes concentrated at internal channels mounds. c) Channel in profile, showing mixed erosive and depositional elements (Type 2).

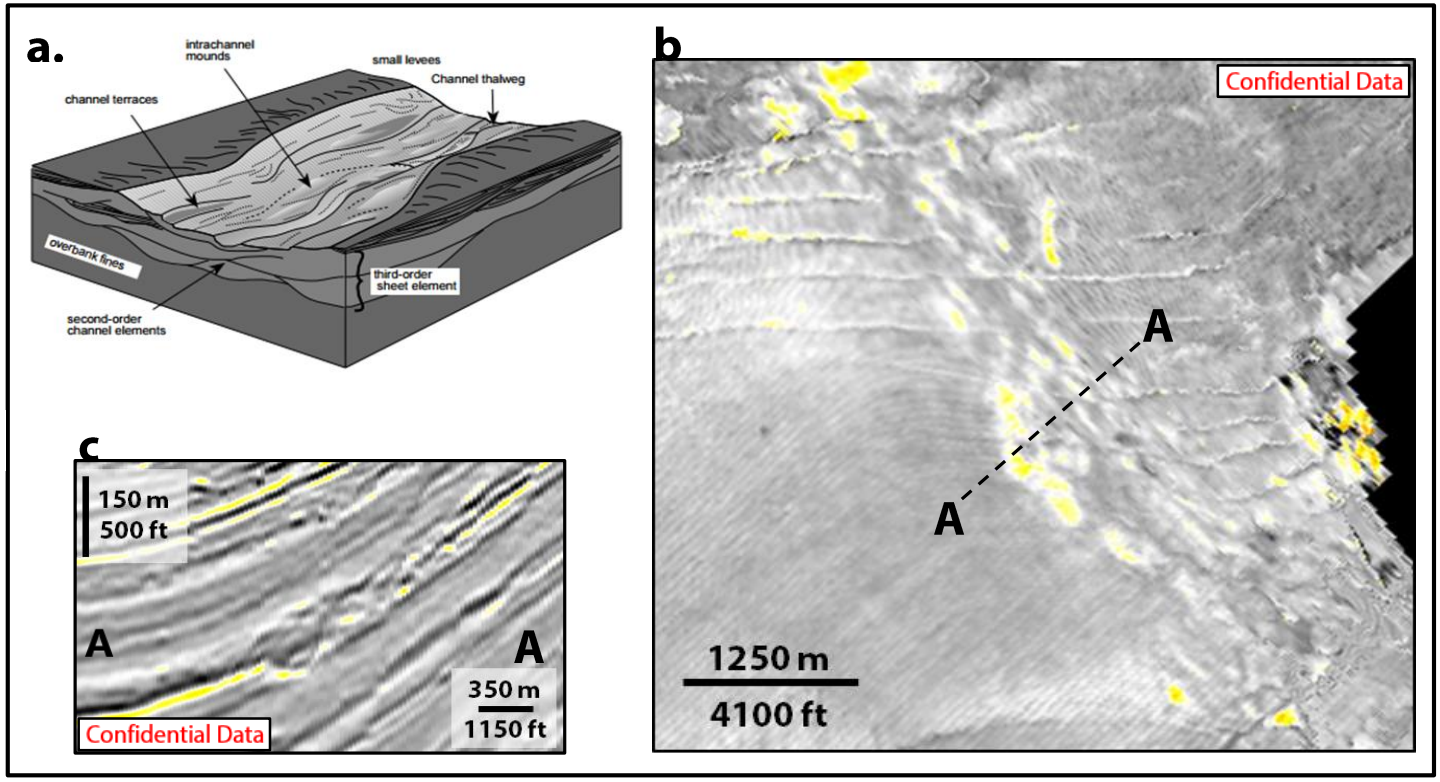

Figure 9. Uninterpreted and interpreted amplitude map of west-to-east flowing distributary system.

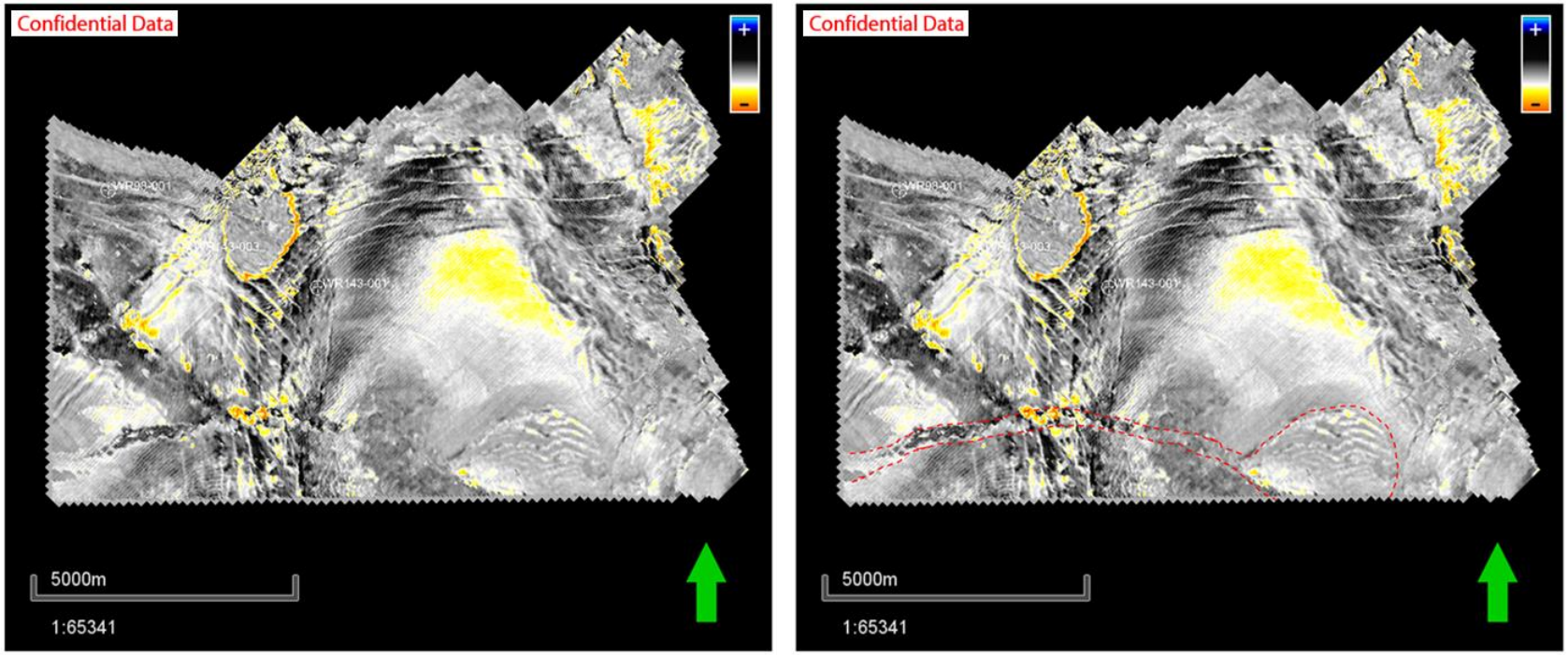

Figure 10. WR98-001 log interpretation. Yellow bars correspond to intervals interpreted as sandier based on low gamma ray and resistivity response; the uppermost interval is the most prominent sand package in all three wells. The inferred BSR depth is shown with a red dashed line. Proximal channel numbers correspond to systems identified in Table 1.

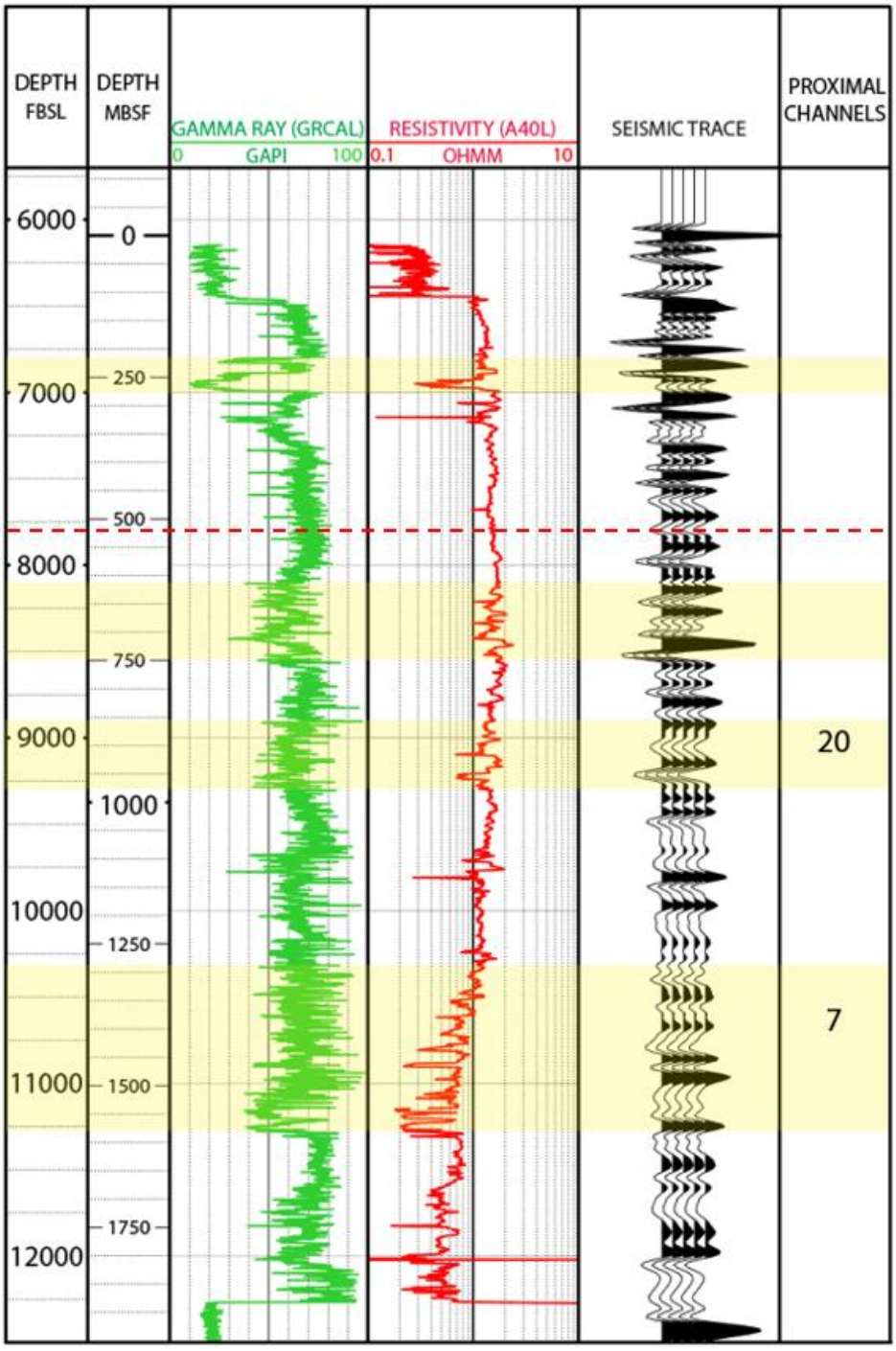

Figure 11. Instantaneous amplitude map corresponding to prominent sand-bearing horizon in WR98-001 (Hrz600). A narrow channel occurs on the eastern side of the dataset, but no channelization is visible in the well area.

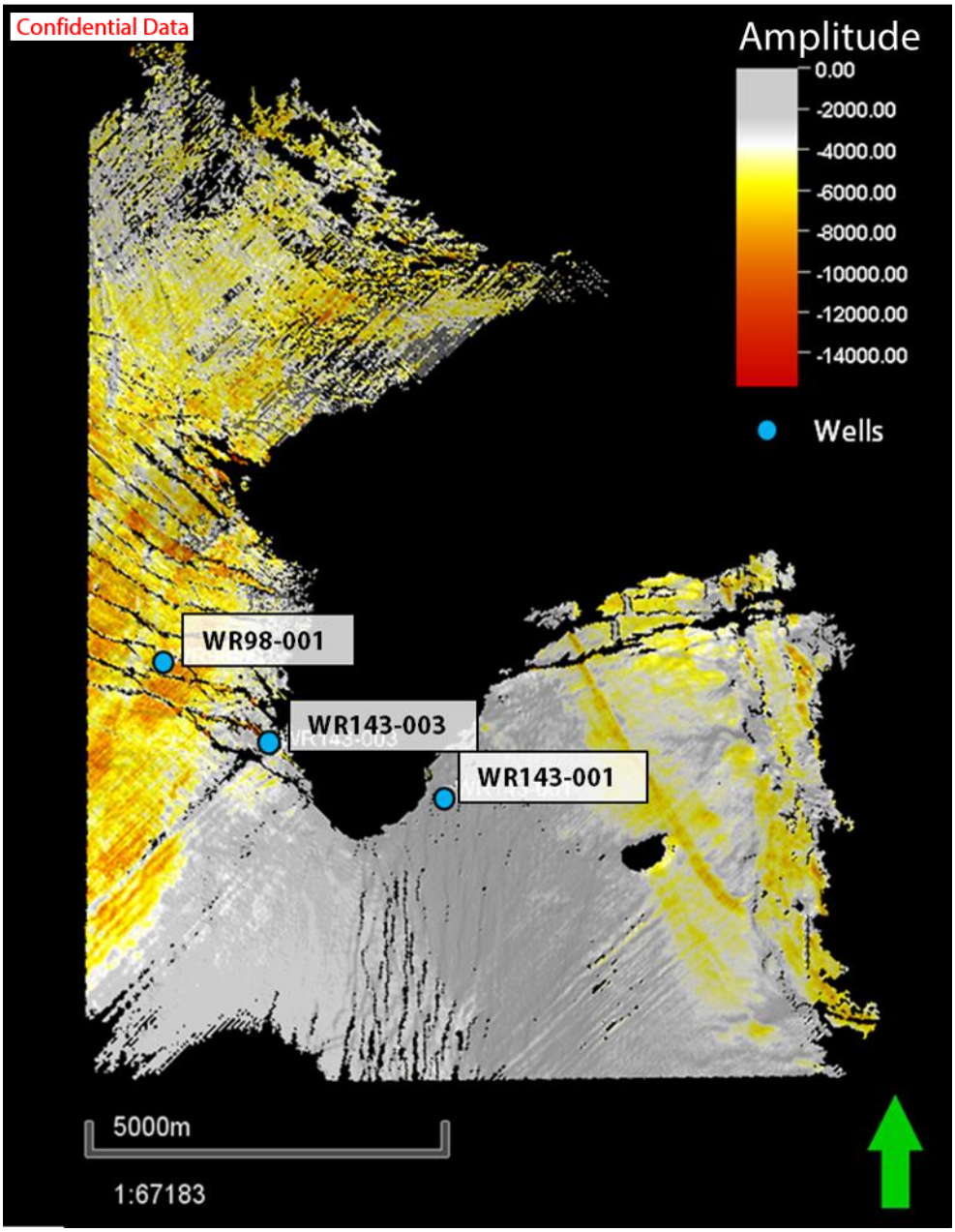

Figure 12. WR143-003 log interpretation. Yellow bars correspond to intervals interpreted as sandier based on low gamma ray and resistivity response; the inferred BSR is shown with a red dashed line. The green bar corresponds to a strong resistivity kick interpreted as gas hydrate bearing-sediments.

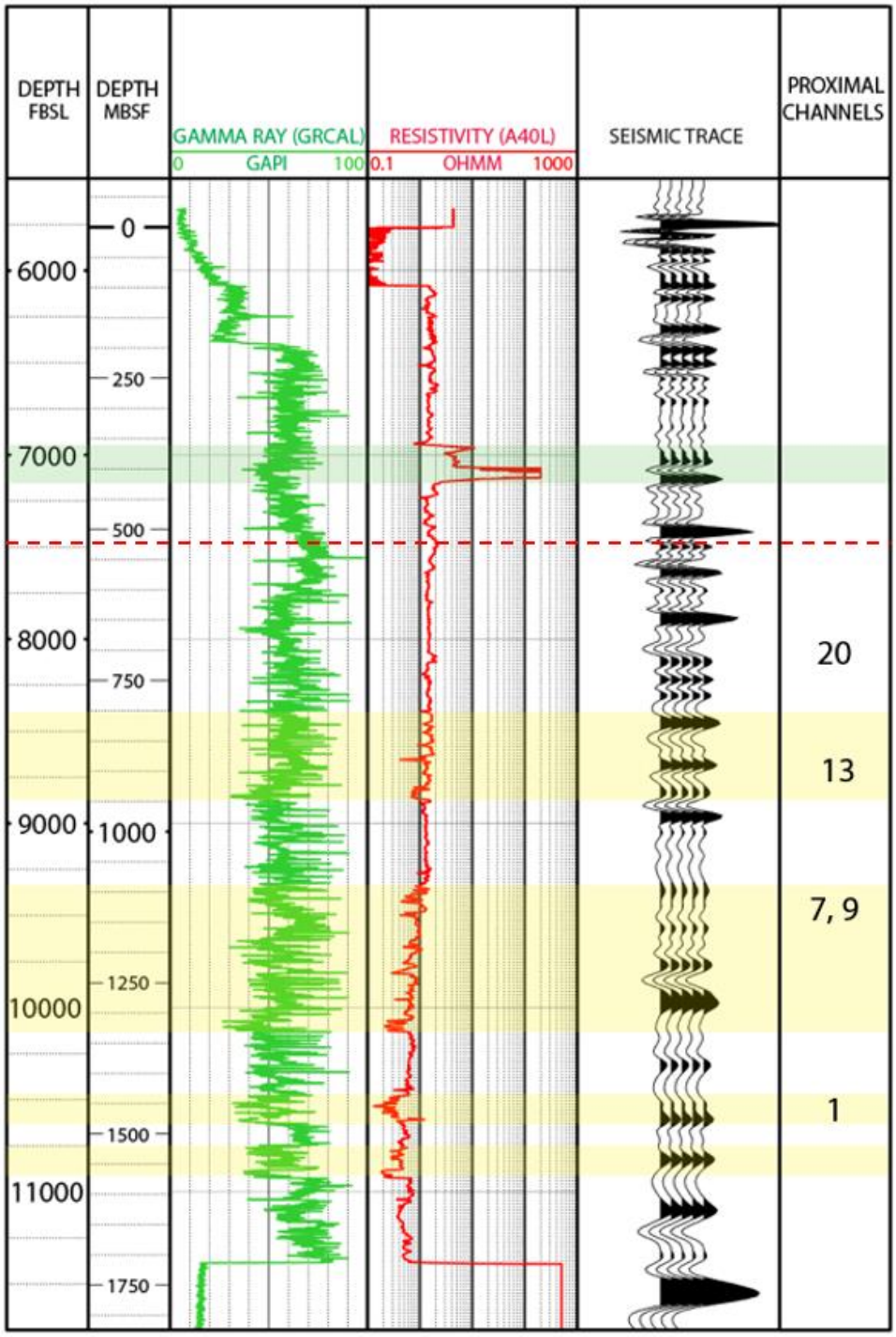

Figure 13. WR143-003 log interpretation. Yellow bars correspond to intervals interpreted as sandier based on low gamma ray and resistivity response; green bars correspond to gas hydrate in fractures based on high resistivity and gamma ray response. The inferred BSR is shown with a red dashed line. The sharp drop in resistivity and gamma ray at 9450 fbsl corresponds to a casing point, immediately below which sands generate a relatively low amplitude seismic response.

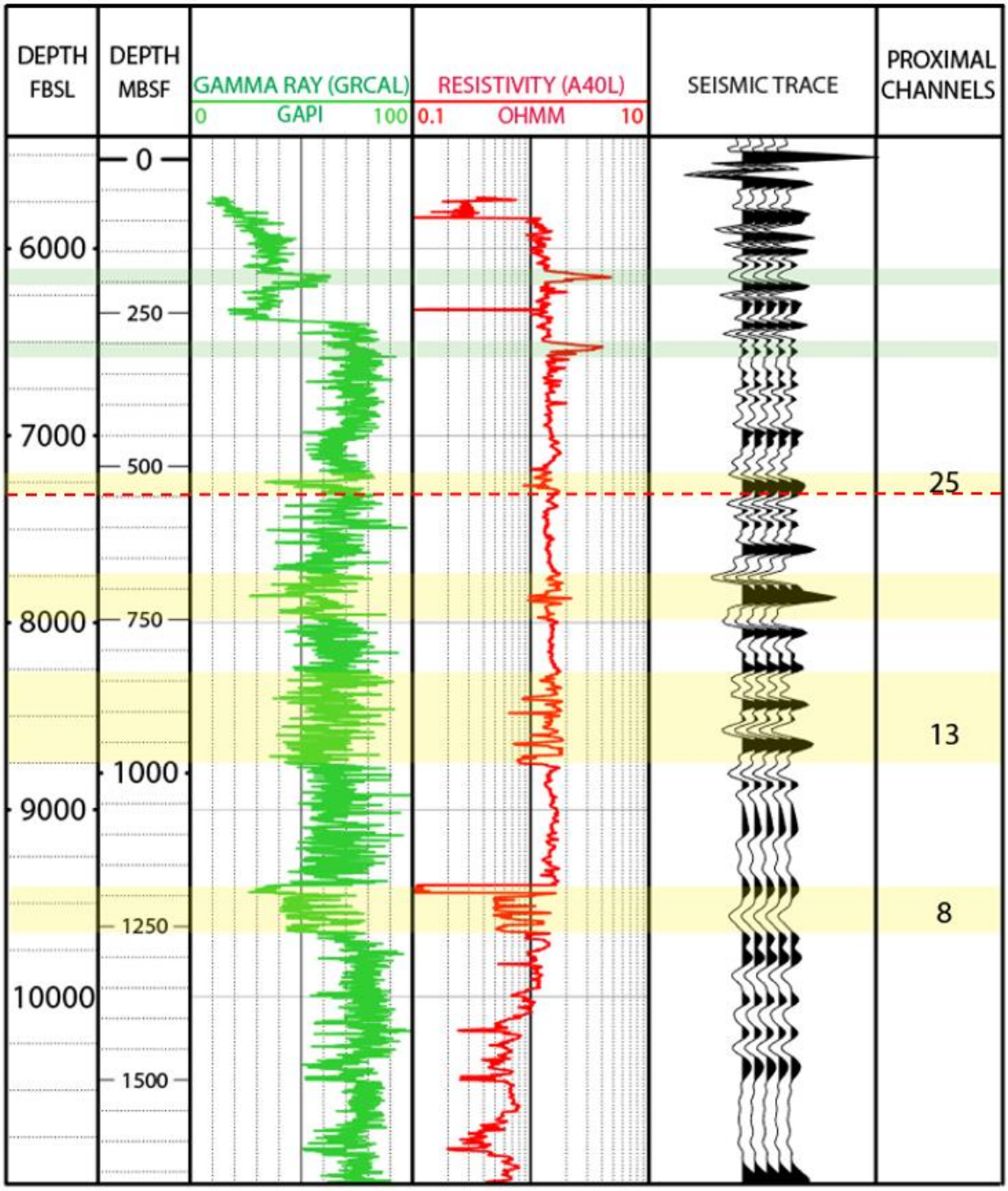

Figure 14. Map of well locations and all channel segments mapped in profile. Wells do not directly penetrate an identified channel, but several systems are proximal and correspond to more permeable intervals in the well logs.

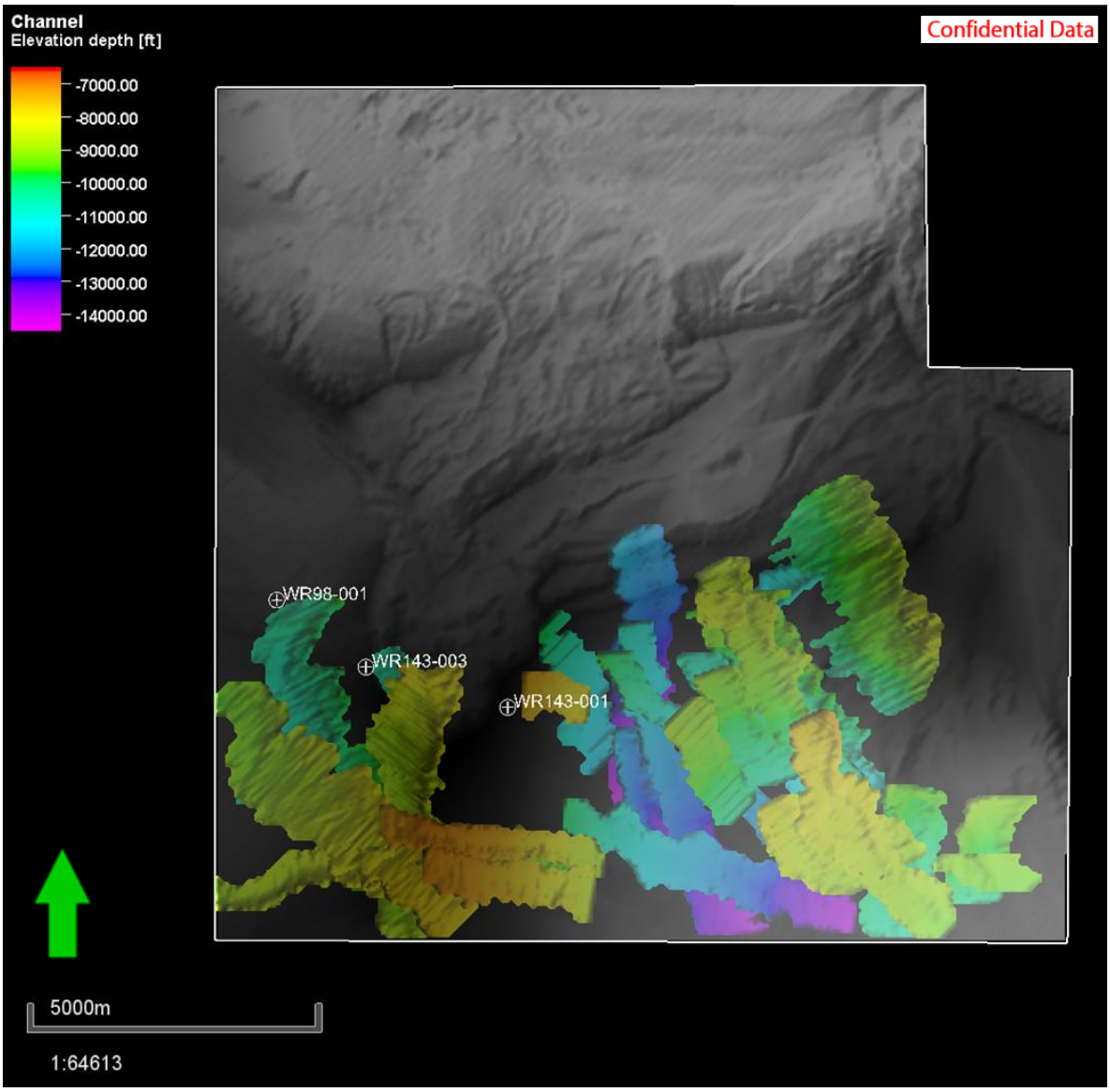

Figure 15. Arbitrary line showing flattened horizons, with shading to lower horizon to highlight thinning and thickening trends. a) Hrz005 (flattened) shaded to Hrz001, b) Hrz100 (flattened) shaded to Hrz005, c) Hrz400 (flattened) shaded to Hrz100, d) Hrz500 (flattened) shaded to Hrz400, e) Hrz750 (flattened) shaded to Hrz500, and f) seafloor (flattened) shaded to Hrz750. Map of seafloor shows arbitrary line location.

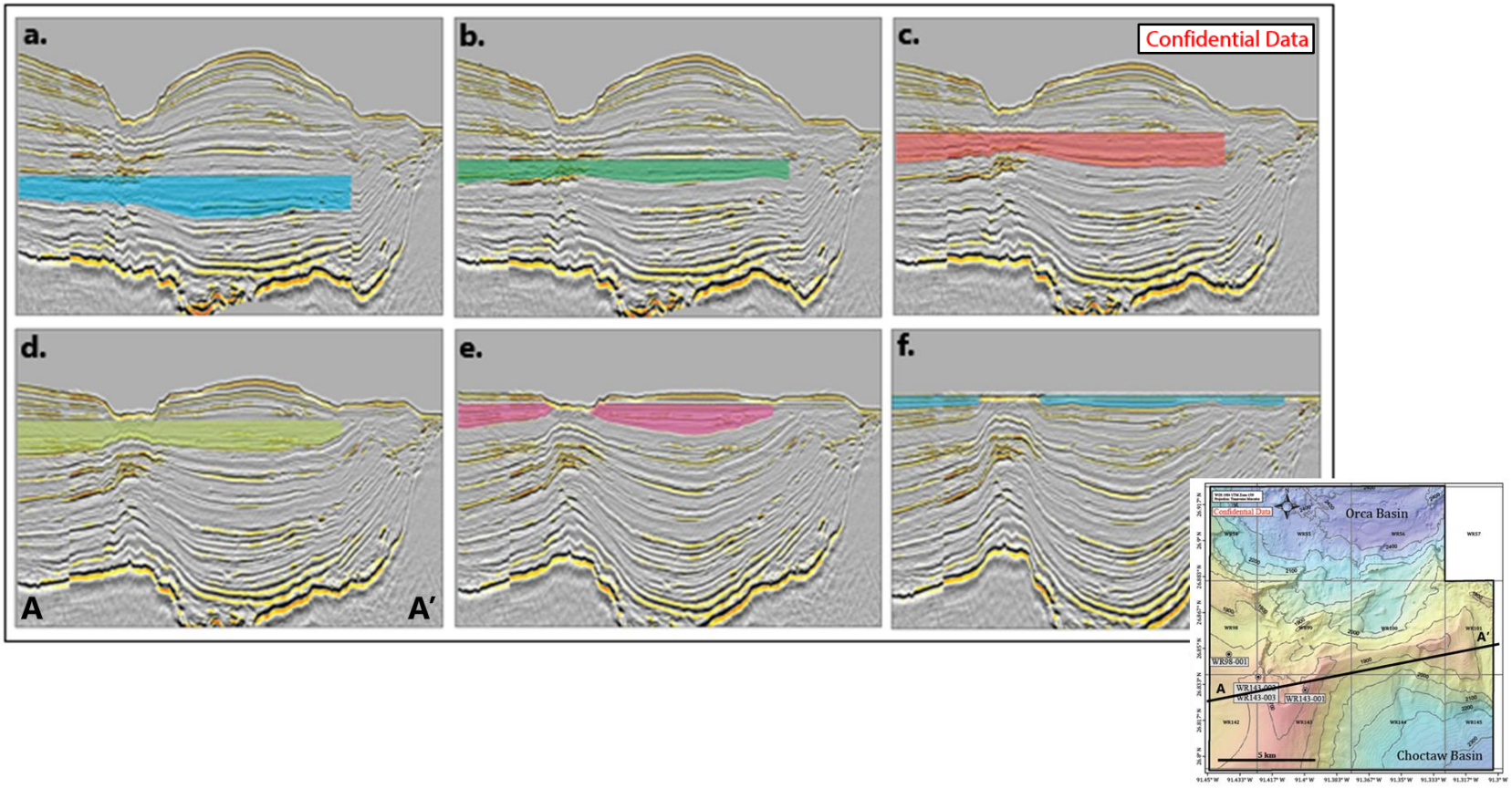

Figure 16. Isopachs of shaded intervals from Figure 15. Scales vary, but in all cases red corresponds to thickest areas and purple to thinnest areas. a) Thickness between Hrz005 and Hrz001, b) thickness between Hrz100 and Hrz005, c) thickness between Hrz400 and Hrz100, d) thickness between Hrz500 and Hrz400, e) thickness between Hrz750 and Hrz500, and f) thickness between seafloor and Hrz750. This interval also shows the prominent slump features associated with seismic Unit 1.

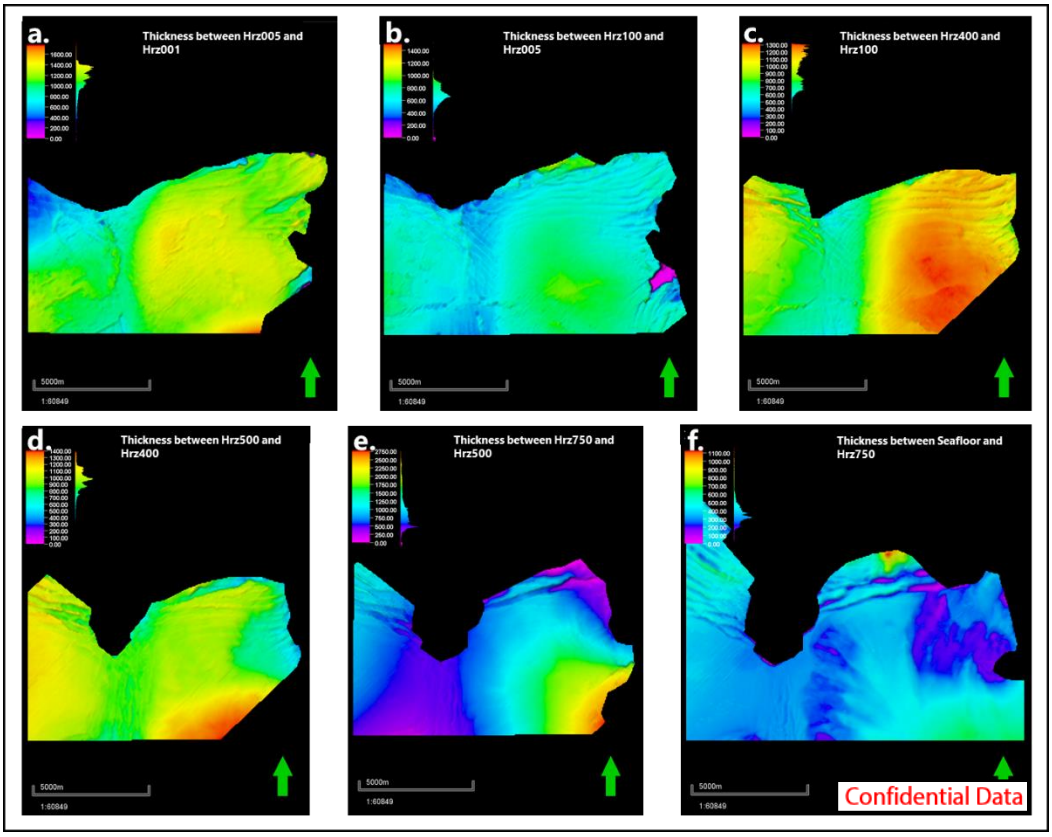

Figure 17. Example of mounding over channel axis. The concave-downward shape indicated by the arrow is caused by the differential compaction of sands and muds. Bright amplitudes also indicate coarse-grained channel fill.